Computation of Domain-Averaged Irradiance Using Satellite-Derived Cloud Properties

SEIJI KATO

Center for Atmospheric Sciences, Hampton University, Hampton, Virginia

FRED G. ROSE

Analytical Services and Materials, Inc., Hampton, Virginia

THOMAS P. CHARLOCK

NASA Langley Research Center, Hampton, Virginia

(Manuscript received 18 March 2004, in final form 30 July 2004)

ABSTRACT

The respective errors caused by the gamma-weighted two-stream approximation and the effective thickness approximation for computing the domain-averaged broadband shortwave irradiance are evaluated using cloud optical thicknesses derived from 1 h of radiance measurements by the Moderate Resolution Imaging Spectrometer (MODIS) over footprints of Clouds and the Earth's Radiant Energy System (CERES) instruments. Domains are CERES footprints of which dimension varies approximately from 20 to 70 km, depending on the viewing zenith angle of the instruments. The average error in the top-of-atmosphere irradiance at a 30° solar zenith angle caused by the gamma-weighted two-stream approximation is 6.1 W m^{-2} (0.005 albedo bias) with a one-layer overcast cloud where a positive value indicates an overestimate by the approximation compared with the irradiance computed using the independent column approximation. Approximately one-half of the error is due to deviations of optical thickness distributions from a gamma distribution and the other half of the error is due to other approximations in the model. The error increases to 14.7 W m^{-2} (0.012 albedo bias) when the computational layer dividing the cloud layer is increased to four. The increase is because of difficulties in treating the correlation of cloud properties in the vertical direction. Because the optical thickness under partly cloudy conditions, which contribute two-thirds of cloudy footprints, is smaller, the error is smaller than under overcast conditions; the average error for partly cloudy condition is -2.4 W m^{-2} (-0.002 albedo bias) at a 30° solar zenith angle. The corresponding average error caused by the effective thickness approximation is 0.5 W m^{-2} for overcast conditions and -21.5 W m^{-2} (-0.018 albedo bias) for partly cloudy conditions. Although the error caused by the effective thickness approximation depends strongly on the optical thickness, its average error under overcast conditions is smaller than the error caused by the gamma-weighted two-stream approximation because the errors at small and large optical thicknesses cancel each other. Based on these error analyses, the daily average error caused by the gamma-weighted two-stream and effective thickness approximations is less than 2 W m^{-2}.

1. Introduction

The reflected shortwave irradiances from clouds vary because of temporal and spatial variations of cloud optical properties. In addition, the resolution of instruments measuring radiation is small enough to detect the variations but not large enough to average them out. For climate purposes, our interest is on an average albedo, transmittance, and absorptance over a finite area or time. Because the albedo and transmittance are not linearly related to cloud optical thickness, those computed using the average optical thickness could be in error. The average optical thickness over a domain is often derived by separating the domain into subgrids and averaging subgrid-scale optical thicknesses weighted by their fractional areas. A better way to obtain the domain-averaged irradiance is by computing the irradiance for all subgrid columns separately. The domain-averaged irradiance is then the average of the subgrid-scale irradiances (the independent column approximation; Cahalan et al. 1994b). The independent column approximation neglects net horizontal exchange of radiation, but it treats vertical and horizontal inhomogeneity of cloud properties within a framework of 1D radiative transfer. The irradiance profile computed with the independent column approximation agrees with that from a three-dimensional radiative

Corresponding author address: Seiji Kato, Mail Stop 420, NASA Langley Research Center, Hampton, VA 23681-2199.
E-mail: s.kato@larc.nasa.gov

transfer algorithm for a variety of clouds ranging from marine stratocumulus clouds (Cahalan et al. 1994b) to violent convective clouds (Oreopoulos and Barker 1999; Barker et al. 2003). Explicitly computing radiation for all columns, however, becomes more computationally expensive as the number of subgrid-scale columns in the domain increases.

Several approximations are possible to avoid explicitly computing radiation for all subgrid-scale columns. Cahalan et al. (1994a) expand the albedo function of subgrid columns expressed as a function of the logarithm of the optical thickness in a Taylor series. Summing all subgrid-albedo functions and neglecting higher-order terms leads to the domain-averaged albedo expressed by the logarithmic mean of cloud optical thicknesses (the effective thickness approximation). Barker (1996) assumes that the cloud optical thickness distribution in a domain follows a gamma distribution. Analytically integrating a two-stream solution over a gamma distribution provides the domain-averaged transmittance and albedo as a function of two parameters of a gamma distribution (the gamma-weighted two-stream approximation). Cairns et al. (2000) derive mean radiation in a statistically isotropic inhomogeneous medium and show that it can be expressed by simply scaling optical properties derived for a homogeneous cloud. All three approximations aim to determine cloud properties that give a sufficiently accurate albedo, transmittance, and absorptance compared with those given by 3D calculations or by the independent column approximation.

One application of these approximations is the computation of the global radiation budget. While the top-of-atmosphere irradiance can be estimated from radiance measurements (e.g., Smith et al. 1986; Loeb et al. 2003), we often need to know the irradiance at the surface or absorption by the atmosphere. Because satellite measurements are limited to top-of-atmosphere radiances and surface observations cannot cover the entire earth, the global irradiance profile and surface radiation budget must rely on radiative transfer models. Irradiances at the top of the atmosphere and surface were computed in earlier studies using satellite-derived cloud properties. Zhang et al. (1995) and Rossow and Zhang (1995) used cloud properties derived for International Satellite Cloud Climatology (ISCCP; Rossow and Schiffer 1991) and computed the longwave and shortwave broadband irradiance in 280 km by 280 km horizontal grids. Their comparison with Earth Radiation Budget Estimate (ERBE; Barkstrom 1984) data shows that the global monthly mean top-of-atmosphere irradiance is approximately 10 W m^{-2} larger than observations (Rossow and Zhang 1995). An intensive local-scale comparison of top-of-atmosphere and surface irradiances shows even larger discrepancies (Charlock and Alberta 1996). These results indicate the need for improved radiative transfer algorithms and for improved observations, especially those used for computations as inputs. These computations, however, do not explicitly include effects of subgrid-scale horizontal inhomogeneity of cloud properties. Rossow et al. (2002) extended the study by Zhang et al. (1995) and estimated the effect of cloud inhomogeneity; including horizontal cloud inhomogeneity reduces the daily global mean top-of-atmosphere irradiance by 15 W m^{-2}, which is regarded as a bias error if one assumes plane-parallel horizontally homogeneous clouds. The method used by Rossow et al. (2002) is an improved effective thickness approximation; therefore, it does not treat distribution of cloud optical thickness explicitly. One could take a different approach by applying the gamma-weighted two-stream approximation in computing irradiance profiles using satellite-derived cloud properties. This method explicitly treats the distribution of cloud optical thickness in computing the radiation budget. Barker et al. (1996) and Oreopoulos and Davies (1998) used satellite-derived cloud properties for single-layer clouds to evaluate the error in albedos by the gamma-weighted two-stream approximation. As pointed out by Oreopoulos and Barker (1999), however, this error depends on the number of computational layers into which a cloud layer is divided. Oreopoulos and Barker (1999) analyzed the error caused by the treatment of multiple-layer clouds using properties generated by cloud resolving models.

In this paper, we use cloud properties derived from satellite data and focus on the computational error in the global radiation budget estimate. Specifically, this study evaluates the error in broadband shortwave irradiances computed using the gamma-weighted two-stream approximation and the effective thickness approximation by comparing these results to the irradiances computed with the independent column approximation. For the analysis, we use a dataset from the Clouds and the Earth's Radiant Energy System (CERES) project (Wielicki et al. 1996). Each domain is a CERES footprint. Retrievals using Moderate Resolution Imaging Spectrometer (MODIS; King et al. 1992) radiances by Minnis et al. (1998) provide cloud property information for each footprint. The following sections start with a description of the CERES data used for this study. We then explain the 1D radiative transfer model developed for this study; the description clarifies various assumptions on which the model is based. We estimate the error caused by two major assumptions associated with the gamma-weighted two-stream approximation. Finally, we compare the error caused by assumptions in the models with the uncertainty in the irradiance caused by uncertainties in the inputs.

2. CERES dataset

CERES instruments on the *Terra* satellite have a footprint size of approximately 20 km at nadir. MODIS,

which is also on *Terra*, measures narrowband radiances from which cloud properties can be derived. The pixel size of MODIS imager is smaller than the CERES footprint; a CERES footprint contains from a few hundred to 20 000 or 30 000 imager pixels depending on the viewing zenith angle of the CERES instruments. We can, therefore, quantitatively determine the spatial variability of cloud properties over a CERES footprint once imager data are collocated with CERES footprints. One CERES data product, the Single Satellite Footprint (SSF), contains retrieved cloud properties from 1-km-resolution MODIS radiances (Minnis et al. 1998). Properties include the linear and logarithmic averages of cloud optical thickness and cloud optical thickness histograms for each CERES footprint. The cloud optical thickness histogram is expressed by the optical thicknesses corresponding to 13 different percentiles of the total population of cloudy subgrid columns (i.e., the optical thickness in the ascending order at 1%, 5%, 10%, . . . , 95%, and 99% of the population). Note that the algorithm by Minnis et al. (1998) classifies a MODIS pixel either clear or overcast by a threshold method assuming a single-layer cloud in the pixel. The cloud fraction estimated over a CERES footprint is approximately the number of cloudy MODIS pixels divided by total number of pixels. In the calculation process pixels are weighted by the point spread function of CERES instruments (Geier et al. 2002). We used an SSF file containing 1 h of CERES measurements taken on 1 March 2001 over regions approximately between 80°N and 50°S and between 45° and 90°W for this study.

3. Gamma-weighted two-stream approximation

The gamma-weighted two-stream approximation assumes that the distribution of cloud optical thickness follows a gamma distribution given by

$$P(\tau; \bar{\tau}, \nu) = \frac{1}{\Gamma(\nu)}\left(\frac{\nu}{\bar{\tau}}\right)^{\nu} \tau^{\nu-1} e^{-\nu\tau/\bar{\tau}}, \quad (1)$$

where $\bar{\tau}$ is the average optical thickness of the layer, and ν is the gamma distribution shape parameter. The solution of the radiative transfer equation with a two-stream approximation is analytically integrated over the gamma distribution from zero to infinity. The accuracy of the gamma-weighted two-stream approximation depends on how closely the actual cloud optical thickness distribution follows the gamma distribution. According to Barker et al. (1996), the mean error in the albedo caused by deviation of the actual distribution from a gamma distribution is less than 0.01 for marine boundary layer clouds. Optical thickness distributions generated by cloud-resolving models for other types of cloud also seem to follow a gamma distribution (Barker and Fu 2000; Oreopoulos and Barker 1999). We further examine cloud optical thickness distributions and the error in the irradiance computations using data taken by *Terra* over oceans that exhibits a wide range of variation of cloud types.

In addition to the error caused by the assumption of a gamma distribution, there is another source of error associated with the gamma-weighted two-stream approximation. When a cloud layer vertically extends through more than one computational layer and the optical thickness distribution in each layer is specified explicitly, the location of the thick or thin parts of the cloud in a subgrid-scale column relative to those in other subgrid-scale columns affects the albedo and transmittance of the domain. As pointed out by Oreopoulos and Barker (1999), when the average irradiance is multiplied by the average albedo or transmittance of the layer, it is equivalent to assuming zero correlation between the cloud properties and incident radiation; all subgrid-scale columns in the lower computational layer receive uniform radiation regardless of the cloud properties directly above them. As a consequence, when an algorithm adopts the gamma-weighted two-stream approximation but neglects vertical correlations, the albedo increases and transmittance decreases with the number of computational layers dividing a cloud layer, approaching their horizontally homogeneous values. If a specific type of cloud overlap is assumed, further complications arise (Barker et al. 2003). The error associated with cloud overlap assumption occurs with both the gamma-weighted two-stream and effective thickness approximations. We, however, do not evaluate the error caused by cloud overlap assumptions in this paper.

On the contrary, the effective thickness approximation does not need to include the vertical correlation of the optical thickness within a cloud layer because it does not explicitly treat the optical thickness distribution. Therefore, two major sources of error unique to the gamma-weighted two-stream approximation are 1) gamma distribution estimate and 2) treatment of the vertical correlation of cloud properties when a single-layer cloud is divided into more than one computational layer. In the following sections, we describe the method to treat these two issues.

a. Gamma distribution estimate

The accuracy of irradiances computed by the gamma-weighted two-stream approximation depends on the method used to estimate two gamma distribution parameters. A straightforward way to estimate these values is to use moments such that the average optical thickness $\bar{\tau}$ is given by $1/n\Sigma_{i=1}^{n}\,\tau_i$ and shape parameter ν is given by $(\bar{\tau}/\sigma)^2$, where σ is the standard deviation of τ. Oreopoulos and Davies (1998) show, however, that the albedo bias is about 0.03 when the moment method is used to estimate the shape parameter. Instead of using the moment method, they suggest the maximum likelihood method by Thom (1958). However, we found

a slightly smaller average error in the albedo if the maximum likelihood method of Greenwood and Durand (1960) is used. Using their method, two parameters are

$$\nu = \frac{0.500\,087\,6 + 0.164\,885\,2D - 0.054\,427\,4D^2}{D}, \tag{2}$$

when

$$0 \le D \le 0.5772,$$

$$\nu = \frac{8.898\,919 + 9.059\,950D - 0.977\,537\,3D^2}{17.797\,28D + 11.968\,477D^2 + D^3}, \tag{3}$$

when

$$0.5772 \le D \le 17.0,$$

where

$$D = \ln\bar{\tau} - \overline{\ln\tau}, \tag{4}$$

$$\bar{\tau} = \frac{1}{n}\sum_{i=1}^{n}\tau_i, \tag{5}$$

$$\overline{\ln\tau} = \frac{1}{n}\sum_{i=1}^{n}\ln\tau_i, \tag{6}$$

and n is the number of overcast subgrid columns.

Based on this method, the logarithmic mean of the average cloud optical thickness, that is, $\exp(\overline{\ln\bar{\tau}})$, at 630 nm is 7.0 when the cloud fraction over a CERES footprint, is 100% (overcast) for the dataset we used in this study. The logarithmic mean of the average cloud optical thickness for all partly cloudy scenes is 3.3. Likewise, the logarithmic mean of the shape parameter, $\exp(\overline{\ln\nu})$, for overcast clouds is 5.2 and for partly cloudy scenes is 2.9 (Table 1).

We also computed $\exp(\overline{\ln\bar{\tau}})$ and $\exp(\overline{\ln\nu})$ from 30 available months of CERES data (Table 1) to check whether the subset of CERES data used in this study is statistically similar to 30 months of CERES data. Although the overcast clouds used in this study are optically thinner and broken clouds are optically thicker than the 30-month average, the subset covers a similar range of $\bar{\tau}$ and ν as compared with 30 months of data (Fig. 1).

TABLE 1. Summary of cloud properties from CERES data. Overlines indicate the average and σ indicates the std dev.

Scene type	$\exp(\overline{\ln\tau})$ ($\sigma_{\ln\bar{\tau}}$)	$\exp(\overline{\ln\nu})$ ($\sigma_{\ln\nu}$)	Fraction to all samples
30 months avg			
Overcast	9.1 (1.0)	5.1 (1.2)	0.32
Partly cloudy	2.2 (0.9)	2.4 (1.2)	0.68
Data used for this study			
Overcast	7.0 (1.0)	5.2 (1.1)	0.39
Partly cloudy	3.3 (1.0)	2.9 (1.3)	0.61

b. *Treatment of vertical correlations in direct irradiance in the radiative transfer model*

We extend the expression derived by Kato (2003) in treating the vertical correlation of cloud properties. The concept of treating the correlation is the same for both the direct and diffuse irradiances. We start with descriptions of the direct irradiance because the mathematical expression is simpler. The vertical profile of the domain-averaged direct irradiance depends on the cloud fraction over the domain, location of subgrid-scale clouds relative to those in above layers, and the extinction coefficient along the path of the direct radiation. The domain-averaged transmittance of the direct irradiance for the cloud layer is

$$\overline{T^d}(\bar{\tau}, \nu) = \int_0^\infty P(\tau; \bar{\tau}, \nu)\exp(-\tau/\mu_0)\,d\tau, \tag{7}$$

where μ_0 is the cosine of the solar zenith angle, P is the probability density function given by (1), and superscript d indicates that the transmittance is for the direct irradiance. The domain-averaged direct irradiance at the cloud base is $\overline{T^d}$ multiplied by the direct irradiance incident on the cloud top.

When the cloud layer is located below another cloud layer, the subgrid column transmittance in (7) needs to be weighted by the incident direct irradiance in addition to the cloud optical thickness distribution because subgrid-scale columns that receive larger than the domain average incident direct irradiance contribute to the direct irradiance at the cloud base more than subgrid columns that receive smaller incident radiation (Oreopoulos and Barker 1999). Subgrid columns below thin clouds receive more direct incident radiation than columns below thick clouds. When a single-layer cloud is simply divided into two computational layers, thicker parts in the lower computational layer, which receive less direct incident radiation, are always below thicker parts in the upper computational layer (Fig. 2). To include this correlation, we assume that the incident direct irradiance F^d on a subgrid-scale column of optical thickness τ is proportional to

$$F^d \propto \exp(-C\tau/\mu_0), \tag{8}$$

where

$$C = \eta\bar{\tau}_u/\bar{\tau}, \tag{9}$$

where $\bar{\tau}_u$ is the average optical thickness of the upper layer, and η is a variable depending on the degree of correlation of the optical thickness of the two cloud layers. Note that C is written in the above form for convenience in the later Eq. (11). The domain-averaged transmittance of the direct irradiance is then

$$\overline{T^d}(\bar{\tau}, \nu) = \left(1 + \frac{\bar{\tau}C}{\mu_0\nu}\right)^{\nu}\int_0^\infty P(\tau; \bar{\tau}, \nu)\exp[-(1 + C)\tau/\mu_0]\,d\tau, \tag{10}$$

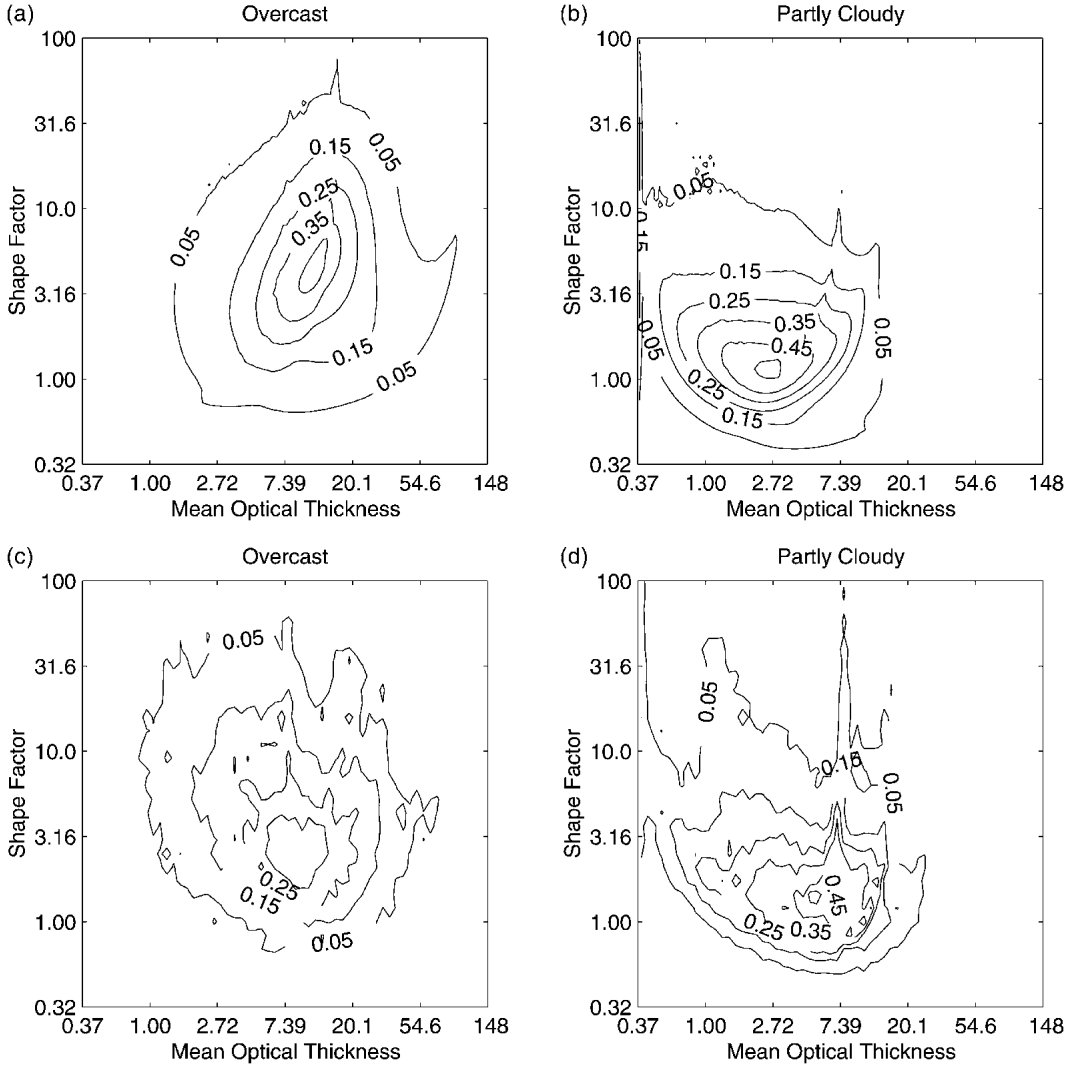

FIG. 1. Contour plot of the number of CERES footprints in the cloud optical thickness and shape parameter bins divided by the width of the bins for overcast and partly cloudy footprints: (a),(b) from available 30 months of CERES data; (c),(d) from the dataset used in this study.

where the term $(1 + \bar{\tau}C/\mu_0\nu)^\nu$ appears in order to normalize the weighting function.

The domain-averaged transmittance of the direct irradiance $\overline{T^d}$ is, therefore,

$$\overline{T^d}(\xi) = \left(\frac{\mu_0\nu + \bar{\tau}C}{\mu_0\nu + \bar{\tau}C + \xi\bar{\tau}}\right)^\nu = \left(\frac{\mu_0\nu + \bar{\tau}_u\eta}{\mu_0\nu + \bar{\tau}_u\eta + \xi\bar{\tau}}\right)^\nu, \tag{11}$$

where ξ varies from 0 at the top of the lower layer and 1 at the bottom of the lower layer. We introduce ξ so that the transmittance is expressed at any level of the layer and changing the mean optical thickness of the layer $\bar{\tau}$ is distinguished from changing the vertical level within the layer. When η goes to zero, (11)

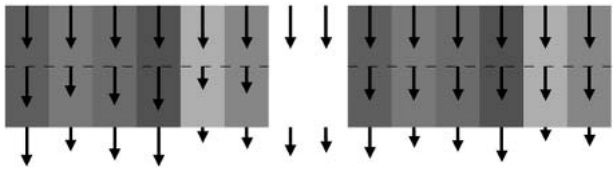

FIG. 2. Schematic diagram of a cloud layer divided by subgrid columns and by two computational layers. Downward arrows indicate the direct irradiance at the top and bottom of the computational layers. Four arrows in the middle of two clouds indicate the average irradiance at the cloud top and base. The left side treats the vertical correlation but the right side assumes that incident irradiance at the top of the lower layer is the same for all subgrid columns. The average irradiance at the cloud base for the left side is greater than that for the right side.

and the domain-averaged irradiance coincide with the irradiance computed with no correlation. When the correlation is perfect (i.e., $\eta = 1$), multiplying (11) by the transmittance of the upper layer $[\mu_0\nu/(\mu_0\nu + \bar{\tau}_u)]^\nu$, which can be derived by applying (7) to the upper layer, agrees with the transmittance of a layer of optical thickness $\bar{\tau}_u + \bar{\tau}$, that is, $[\mu_0\nu/(\mu_0\nu + \bar{\tau}_u + \bar{\tau})]^\nu$.

The above argument for two layers can be extended to $N + 1$ layers when $\Sigma_{j=1}^{N} \bar{\tau}_j$ is substituted for $\bar{\tau}_u$, where N is the number of cloud layers above the lower layer. However, we need to derive an expression for η such that the correlation between the lower layer and all other layers above it can be treated using observable cloud properties. To derive the expression, we start with a general cloud field in which cloud amounts vary with height. Suppose we are interested in the direct irradiance at the bottom of the ith layer, which is located below layer j. Because correlation depends on both the position of clouds and their extinction coefficients, C in (8) is divided into two parts such that

$$C_{ij} = \sum_{j=1}^{N} \{[P(A_j|A_i) - A_j] + P(A_j|A_i)\mathcal{R}(\beta_j, \beta_i)\} \frac{\bar{\tau}_j}{\bar{\tau}_i}, \tag{12}$$

where A_j is the cloud fraction in the jth layer, and $P(A_j|A_i)$ is the probability of cloud occurrence in the jth layer of a subgrid column provided the ith layer in the subgrid column is cloudy—that is, the number of subgrid columns with clouds in both the jth and ith layers divided by the number of subgrid columns that have clouds in the ith layer. The summation in (12) is necessary to account for all combinations between the ith layer and layers above it. The first two terms that are in the brackets describe the departure of the cloud overlap probability from random overlap. The third term accounts for the correlation of the extinction coefficient between cloud layers; $\mathcal{R}(\beta_j, \beta_i)$ depends on the extinction coefficient correlation between the two layers. This leads to $\eta_{ij} = P(A_j|A_i) - A_j + P(A_j|A_i)\mathcal{R}(\beta_j, \beta_i)$.

The cloud retrieval algorithm of Minnis et al. (1998) detects clouds and classifies each subgrid column (pixel) as either clear or overcast. Therefore, when a CERES footprint is separated by a clear and cloudy part, subgrid-scale columns in the clear part do not contain any clouds and those in the cloudy part contains an overcast cloud. Although individual subgrid columns contain only a single-layer overcast cloud, the SSF product allows up to two cloud layers per CERES footprint. When two-layer clouds are present in a footprint, they are nonoverlapping. We assume that all clouds are single layered in this study. When a cloud layer is divided into more than one computational layer $A_j = 1$, $P(A_j|A_i) = 1$ in (12) provided there is only one cloud layer present in a footprint or the irradiances for columns containing nonoverlapping clouds at two heights are computed separately. In addition, the subgrid-scale extinction coefficient is perfectly correlated in the vertical direction because the retrieval assumes a single-layer cloud, hence $\mathcal{R}(\beta_j, \beta_i) = 1$. Therefore, $\eta_{ij} = 1$ and

$$C_{ij} = \frac{\bar{\tau}_j}{\bar{\tau}_i}. \tag{13}$$

c. *Treatment of vertical correlations in diffuse irradiance*

Following Oreopoulos and Barker (1999), we express the diffuse incident irradiance in an exponential form $\exp[-0.063C\tau(2 - \mu_0)]$, where C is given by (9), so that an analytical expression can be derived. The treatment of the correlation is the same as that for the direct irradiance; a two-stream solution weighted by the cloud optical thickness distribution and incident diffuse irradiance is integrated from 0 to infinity (appendix A). Because the delta approximation (Joseph et al. 1976) retains the forward scattered light in the direct beam, C needs to be adjusted slightly (appendix B) in computing the diffuse irradiance. We assume that all subgrid columns receive uniform incident diffuse irradiance at the boundaries when a cloud is in one computational layer.

4. Irradiance computation

We compute four sets of broadband shortwave irradiance vertical profiles per footprint using different approximations. The first method explicitly computes the irradiance 13 times using a cloud optical thickness histogram from a CERES footprint in the SSF product. These results are averaged using the fraction of populations in each bin as a weight, which is equivalent to the independent column approximation (hereafter SSF_{13}). When two cloud layers are present in a footprint, we use the distribution of cloud optical thickness from the layer that has a larger fractional area and assume a single-layer cloud. We neglect the clear-sky portion of a footprint for partly cloudy cases to concentrate on estimating the error under cloudy conditions. In other words, the cloud cover is assumed to be 100% even when clouds partly cover a footprint. Therefore, this method requires up to 13 computations per CERES footprint. The second method uses the gamma-weighted two-stream approximation (GWTSA) described in the previous sections. Two gamma distribution parameters are derived from retrieved cloud properties using the method of Greenwood and Durand (1960). While $\bar{\tau}$ retrieved at 645 nm is converted to the optical thickness at other wavelengths, the shape parameter is wavelength independent in this study. The second method requires one computation per CERES footprint. The third method uses the effective thickness approximation (ETA). This method also requires one computation per CERES footprint. The fourth method also uses 13 cloud optical thicknesses from the histo-

gram. Instead of using the satellite-derived optical thickness, it uses the optical thicknesses derived from the gamma distribution corresponding to the 13 percentiles of populations used for SSF_{13}. It then uses the independent column approximation in computing irradiance (Γ_{13}). Therefore, when the irradiances from SSF_{13} and Γ_{13} differ, the difference is caused by the departure of the actual optical thickness distribution from a gamma distribution. We consider the irradiance profile from SSF_{13} the truth in this study. Therefore, the error in the results from the other three methods is considered to be the difference between the irradiance calculated by these methods and that obtained using SSF_{13}.

The midlatitude summer standard atmosphere (McClatchey et al. 1972) is used for all computations in this study. We assume that all clouds are water clouds and use a parameterization by Hu and Stamnes (1993) for a 10-μm cloud particle to compute the optical property of cloud particles. The *k*-distribution method described by Kato et al. (1999) with the correlated-*k* assumption provides the estimate of the gaseous absorption optical thickness of water vapor, ozone, carbon dioxide, and oxygen. The surface albedo is set to 0.06 for all wavelengths, which is approximately the albedo of oceans averaged over the solar spectrum.

5. Results

We use 75 806 CERES footprints that include partly cloudy and overcast scenes. Among those footprints, 29 300 footprints (39%) contain overcast clouds and the remaining 46 506 (61%) footprints are partly cloudy. We use two different solar zenith angles (30° and 60°) for computations, but most of the results presented here are for 30° cases because the results are qualitatively similar. In the first set of computations, a cloud layer is located between 1 and 2 km so that the clouds are always contained within one computational layer. Note that even though retrieved clouds in data are in different heights, we assume that clouds are between 1 and 2 km to avoid a complication to interpreting the results. The first set of computations is, therefore, to test whether actual cloud distributions follow a gamma distribution and to estimate the error in the irradiance. The second set of computations includes a cloud layer extending from 1 to 5 km to estimate the error caused by the correlation treatment.

Figure 3 shows the difference in the top-of-atmosphere upward irradiance between GWTSA and SSF_{13} for overcast cases at a 30° solar zenith angle using the first set of clouds. The error in the GWTSA results increases with average optical thickness. The irradiance difference between GWTSA and Γ_{13} results (2.8 W m^{-2}) accounts for the half of this error and the difference between Γ_{13} and SSF_{13} (3.3 W m^{-2}) accounts for the other half of this error (6.1 W m^{-2}). The difference between Γ_{13} and SSF_{13} is caused by deviations from a gamma distribution in the cloud optical thickness. While approximations in the model such as the assumption of uniform diffuse incident radiation at the cloud boundary for all subgrid columns cause the difference between GWTSA and Γ_{13}, part of the difference between the irradiances is caused by the maximum optical thickness in Γ_{13}. The maximum optical thickness retrieved by Minnis et al. (1998) cloud algorithm is either 128 or 68 depending on approximations in the algorithm. This is the upper limit of the distribution in Γ_{13} and SSF_{13}. In contrast, the analytical solution used for the gamma-weighted two-stream approximation is derived by integrating a two-stream solution from the optical thickness zero to infinity. Therefore, as the average optical thickness increases, the population above the maximum optical thickness in the gamma distribution increases. As a consequence, the top-of-atmosphere irradiance computed with the gamma-weighted two-stream approximation is larger than that with the independent column approximation when the mean optical thickness is close to the maximum optical thickness in the retrieval. This error can be avoided by using incomplete gamma functions (appendix C).

Because of the way the histogram in the SSF product is computed, when most of the retrieved cloud optical thicknesses are the maximum values of the cloud retrieval algorithm and the rest of pixels have much smaller optical thicknesses, the last bin of the histogram represents a wide range of optical thickness; an example is shown in Fig. 8b. In those cases SSF_{13} is close to the effective thickness approximation because the broad bin is weighted heavily and the optical thickness for the bin is computed by logarithmic averaging the upper and lower end of the optical thickness of the bin. To check the effect of footprints containing problematic histograms on the irradiance computations under overcast conditions, we eliminated those footprints having a bin containing more than 16% of all samples. When these footprints are eliminated, the average error of the top-of-atmosphere irradiance in the GWTSA results reduces to 2.3 W m^{-2} at 30° solar zenith angle and to 1.9 W m^{-2} at 60° solar zenith angle (Table 2 in the row labeled "selected footprints").

Figure 3 also shows that the gamma-weighted two-stream approximation produces smaller error over a wider range of optical thicknesses than the effective thickness approximation; the effective thickness approximation performs better in a small range of optical thicknesses around 8 (5 for the 60° solar zenith angle). The average error in the GWTSA overcast case results is 6.1 and 4.0 W m^{-2} for the 30° and 60° solar zenith angle, respectively (Table 2). The corresponding average errors in the ETA overcast results are 0.5 and 3.9 W m^{-2}. The error in the GWTSA results as well as the difference between Γ_{13} and SSF_{13} results are greater than 20 W m^{-2} when the shape parameter ν is less than 1 (not shown in the figures), which indicates that the

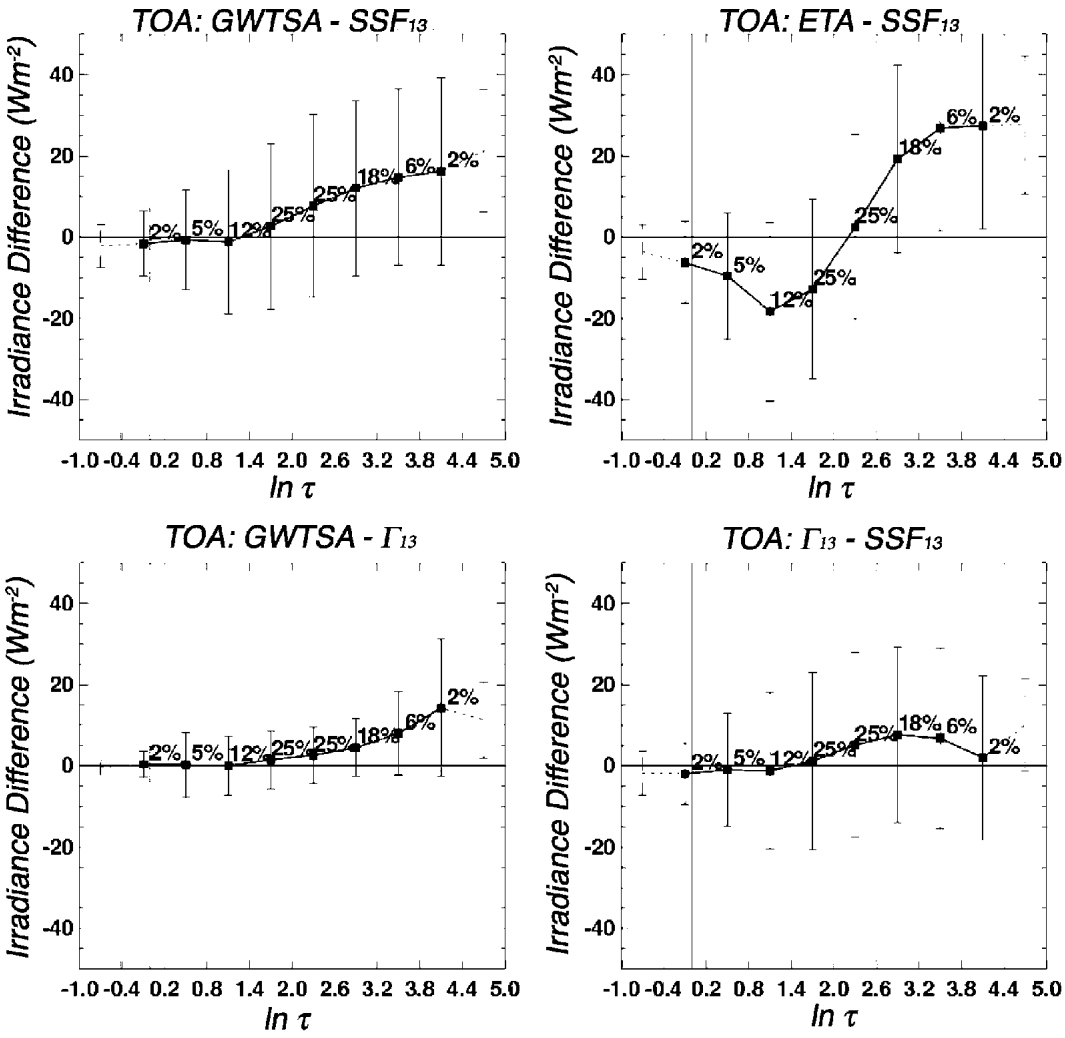

FIG. 3. Top-of-atmosphere irradiance difference for overcast cases computed over CERES footprints as a function of average optical thickness. The solar zenith angle is 30°. The cloud optical thicknesses are derived from MODIS radiances and averaged over a CERES footprint. All clouds are placed between 1 and 2 km. GWTSA and ETA indicate results by the gamma-weighted two-stream approximation and effective thickness approximation, respectively. The methods SSF_{13} and Γ_{13} use the independent column approximation. The error bar indicates the standard deviation and the numbers in the figure indicate the percentage of the population.

cloud optical thicknesses deviate significantly from a gamma distribution when the distribution is extremely broad. The distribution is sometimes bimodal for these cases, indicating that multilayer clouds or both ice and liquid water phase clouds may be present in a footprint. Note that retrieved optical thickness changes by nearly a factor of 2 depending on cloud particle phase assumed. The population of footprints having a shape parameter less than 1 is approximately 5% of footprints in both the data used in this study and the full 30 months of CERES data.

The agreement between GWTSA and SSF_{13} results for partly cloudy cases is better than for overcast cases (Fig. 4). The average error is -2.4 W m^{-2} for the 30° solar zenith angle and it is negligible for the 60° solar zenith angle (Table 2). Because clouds in partly cloudy scenes, which are either broken clouds or edge of clouds, are optically thinner than overcast clouds (Fig. 1 and Table 1), the maximum optical thickness in the cloud retrieval does not affect partly cloudy results as much as overcast results. The absolute difference of the irradiance in the Γ_{13} and SSF_{13} is similar for both the overcast and partly cloudy cases, which indicates that the deviation from a gamma distribution affects the irradiance to a similar degree in both cases. The average error in the partly cloudy ETA results is -21.5 and -8.2 W m^{-2} for solar zenith angles of 30° (Fig. 4) and 60°, respectively (Table 2).

When all overcast and partly cloudy footprints are averaged using the fraction of these cases to all the cases as a weight, the average error in the irradiance computed using the gamma-weighted two-stream ap-

TABLE 2. Summary of errors in irradiance computations. Numbers in parentheses are std dev. The difference for partly cloudy cases is converted to the equivalent value for a 100% cloud cover. Results indicated by selected footprints are those with footprints that contain no bin of the optical thickness histogram having the sample fraction greater than 16%.

Scene type	GWTSA − SSF_{13}	ETA − SSF_{13}	GWTSA − Γ_{13}	Γ_{13} − SSF_{13}
TOA	$\theta_0 = 30°$	one-layer cloud		
Overcast	6.1 (21.1)	0.5 (26.8)	2.8 (8.1)	3.3 (21.3)
Selected footprints	2.3 (15.7)	−2.2 (22.1)	1.3 (4.1)	1.0 (15.9)
Partly cloudy	−2.4 (19.9)	−21.5 (26.9)	−0.1 (6.2)	−2.3 (19.3)
TOA	$\theta_0 = 60°$	one-layer cloud		
Overcast	4.0 (11.0)	3.9 (12.9)	3.0 (5.0)	1.0 (11.4)
Selected footprints	1.9 (8.1)	2.2 (10.0)	1.7 (2.5)	0.2 (8.7)
Partly cloudy	0.0 (12.3)	−8.2 (15.0)	1.6 (4.1)	−1.6 (11.9)
SFC	$\theta_0 = 30°$	one-layer cloud		
Overcast	−7.5 (24.7)	−1.2 (31.2)	−3.8 (9.6)	−3.7 (24.9)
Selected footprints	−3.8 (18.4)	2.1 (25.6)	−1.9 (4.8)	−1.1 (18.7)
Partly cloudy	2.3 (23.6)	24.8 (31.5)	−0.4 (7.4)	2.8 (22.9)
SFC	$\theta_0 = 60°$	one-layer cloud		
Overcast	−4.3 (12.3)	−4.1 (14.4)	−3.2 (5.6)	−1.2 (12.8)
Partly cloudy	0.2 (13.7)	9.4 (16.6)	−1.5 (4.6)	1.8 (13.2)
TOA	$\theta_0 = 30°$	four-layer cloud		
Overcast	14.7 (25.3)	0.4 (28.3)	11.2 (10.8)	3.5 (22.4)
Partly cloudy	1.1 (23.5)	−22.3 (28.1)	3.5 (9.4)	−2.4 (20.2)
SFC	$\theta_0 = 30°$	four-layer cloud		
Overcast	−17.3 (28.6)	−1.4 (31.3)	−13.6 (12.7)	−3.8 (25.3)
Partly cloudy	2.8 (22.9)	24.4 (31.5)	−4.1 (11.0)	−1.3 (26.7)

proximation is 0.9 and 2.5 W m^{-2} (0.0008 and 0.004 albedo bias) at solar zenith angles of 30° and 60°, respectively. Corresponding average errors in the irradiance computed using the effective thickness approximation are −13.1 and −3.5 W m^{-2} (−0.01 and −0.003 albedo bias). Note that the actual average error under all sky conditions is expected to be smaller because the error under partly cloudy conditions is multiplied by the cloud fraction. The magnitude of the average error by the effective thickness approximation is similar to that obtained by Oreopoulos and Davies (1998); their results show that the albedo bias is less than 0.01 with a standard deviation of 0.02–0.04 when the solar zenith angle is approximately 60°.

To understand the error caused by the correlation treatment, we check the sensitivity of the irradiance to a change in the number of computational layers dividing a cloud layer. We increase the number of computational layers from 1 to 10 for clouds with optical thickness varying from 0.1 to 400. We fix the cloud top height at 10 km and extend the base from 9 km for a 1-layer cloud to the surface for a 10-layer cloud. The shape parameter ν is one for all cases. Because retrieved cloud properties using satellite data provide a cloud-top height and we need to check the error as a function of cloud base, we chose this method instead of increasing the number of computational layer with fixed cloud boundaries.

When $\exp(\overline{\ln\tau})$ is less than about 3, the irradiance is insensitive to the number of computational layers (Fig. 5). The maximum change occurs at $\exp(\overline{\ln\tau}) \approx 20$ to 40; the maximum error at a 30° solar zenith angle is approximately 20 W m^{-2} for a 4-layer cloud and more than 35 W m^{-2} for a 10-layer cloud. The maximum moves toward a larger optical thickness with increasing number of layers. Actual clouds with an optical thickness of 40, however, are unlikely to extend 10 km in depth. Figure 5 also shows the empirically estimated physical cloud depth by Minnis et al. (1998) to indicate a typical cloud depth as a function of $\bar{\tau}$. The algorithm predicts 4–6 km for the depth of mid- to high-level clouds when the optical thickness is about 40. Therefore, the typical error using the gamma-weighted two-stream approximation is 20–25 W m^{-2} for the solar zenith angle of 30° and 5–10 W m^{-2} for 60° when a cloud layer is divided by 1-km-thick computational layers and the optical thickness is in a range of about 20–30.

Figure 5 also indicates that the decrease in the surface irradiance almost offsets the increase the top-of-atmosphere irradiance, which implies that the absorption estimate is less affected when the number of computational layers is increased. The difference between the irradiance absorbed by the atmosphere using a one-layer cloud and a five-layer cloud is less than 5 W m^{-2} at a 30° solar zenith angle (Fig. 6a). Increasing the number of cloud layers does not affect the absorption estimated with the gamma-weighted two-stream approximation very much. The absorption estimated with the effective thickness approximation is more affected by the increase (Fig. 6b).

Similar to the error estimate for one-layer clouds, we use the same set of data but place a 4-km-thick cloud between 1 and 5 km so that four computational layers divide a cloud layer. This is to estimate the error caused by the vertical correlation treatment using retrieved cloud optical thickness distribution. The error increases mostly at $\bar{\tau}$ around 15 (Fig. 7 compared with Fig. 3),

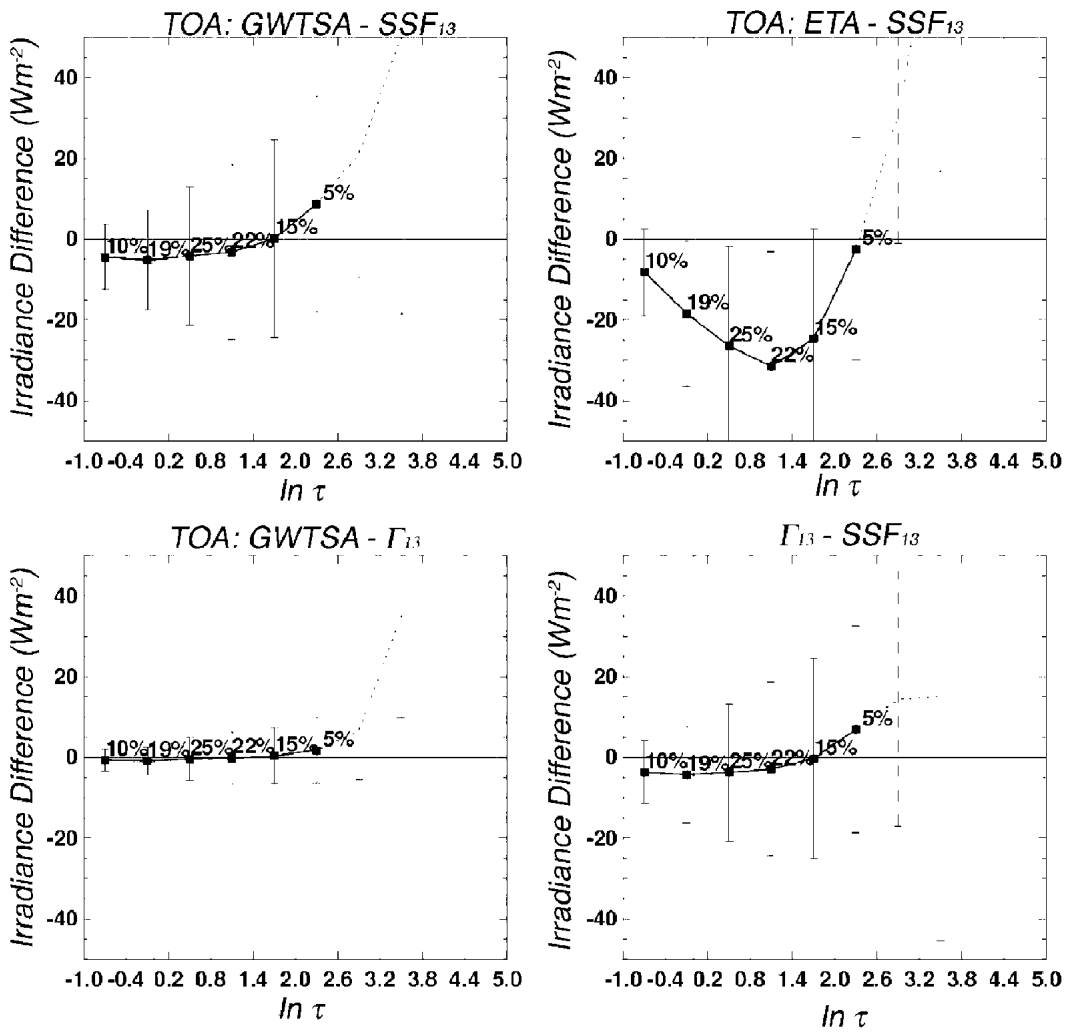

FIG. 4. Same as in Fig. 3, but for partly cloudy cases.

which agrees with the four-layer cloud shown in Fig. 5. The average error in the GWTSA results increases to 14.7 W m^{-2} for overcast cases with the solar zenith angle of 30°. The change in the irradiance caused by increasing from one to four layers for overcast cases is 8.6 W m^{-2}, which is considered to be the average error caused by the approximate correlation treatment used in the model. The average error in the GWTSA results does not increase very much for partly cloudy cases (Fig. 7 compared with Fig. 4) because these clouds are optically thinner than overcast clouds; the average error is 1.1 W m^{-2}. This also agrees with the results in Fig. 5, which shows that the irradiances from thinner clouds are insensitive to the number of computational layers.

6. Discussion

Two sources of error in computing the irradiance profile with the gamma-weighted two-stream approximation considered in the previous section are 1) deviation of actual cloud optical thickness distribution from a gamma distribution, and 2) treatment of vertical correlations of cloud optical thickness when a cloud layer extends through more than one computational layer. These errors are direct consequences of the assumption of a specific distribution of cloud optical thicknesses. In addition, the maximum optical thickness of the retrieval algorithm affects the error caused by the gamma-weighted two-stream approximation in two ways. First, the gamma-weighted two-stream approximation integrates the cloud optical thickness from zero to infinity while retrieved distributions have a maximum. Second, when a footprint contains a large number of pixels with optical thicknesses close to the maximum value and the rest of pixels contain optically thin clouds, the last bin of the histogram covers a very wide range of optical thickness. Figure 8b shows an example of such a histogram along with an example of a prob-

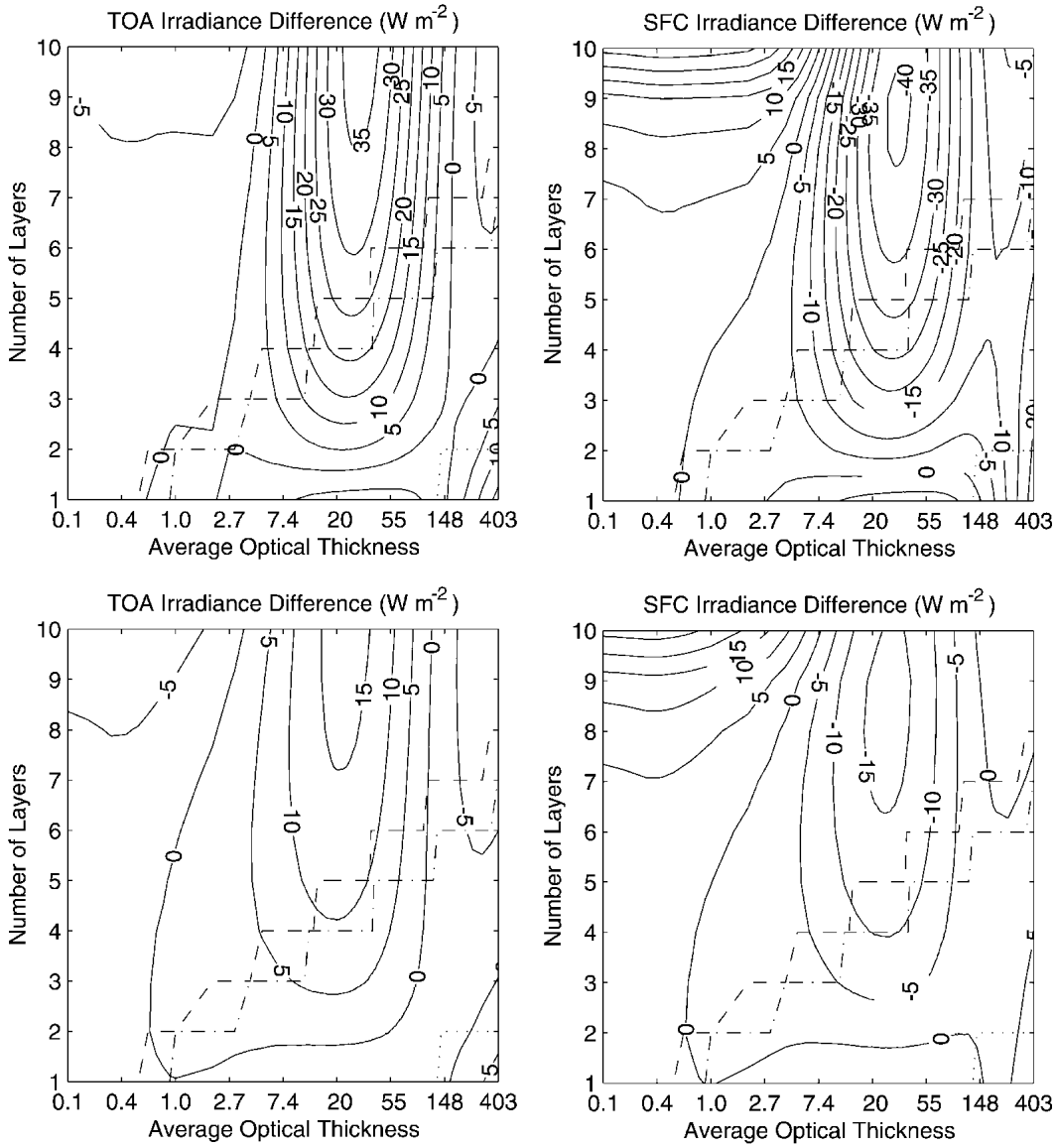

FIG. 5. Contour plot of the error caused by the gamma-weighted two-stream approximation as a function of (natural logarithmic of) the average optical thickness and number of computational layers dividing a cloud layer. Top two plots are for the solar zenith angle of 30° and bottom two plots are for 60° with the surface albedo of 0.06. The cloud top is fixed at 10 km. The cloud base is changed depending on the number of 1-km-thick computational layers. The dashed, dashed–dotted, and dotted lines indicate the empirically estimated number of cloud layers by Minnis et al. (1998) for high-, mid-, and low-level clouds when clouds are divided into 1-km-thick layers.

ability density function of a gamma distribution that agrees with a histogram (Fig. 8a). The last bin of the Fig. 8b case includes the optical thicknesses from 34 to 128 while all subgrids in the bin contain clouds with an optical thickness of 128. For this case, 40% of the subgrid columns in the footprint contain a cloud with τ = 128. The SSF_{13} method then becomes close to the effective thickness approximation because the optical thickness of the last bin is obtained by averaging the logarithm of the upper and lower optical thicknesses of the bin {i.e., exp[(ln34 + ln128)/2] = 66 for the case in Fig. 8b} and the bin is weighted by 0.4 in computing the irradiance for the footprint. Our results indicate that the average error in the top-of-atmosphere irradiance caused by deviations from the actual distributions is 3.3 (1.0) W m^{-2} at a solar zenith angle of 30° (60°), which corresponds to an albedo bias of 0.003–0.004. The effect of the maximum retrieved cloud optical thickness on the top-of-atmosphere irradiance is 2.8 (3.0) W m^{-2} for a 30° (60°) solar zenith angle. When footprints are selected so that artifacts caused by the method obtaining the histogram are eliminated, the average error caused

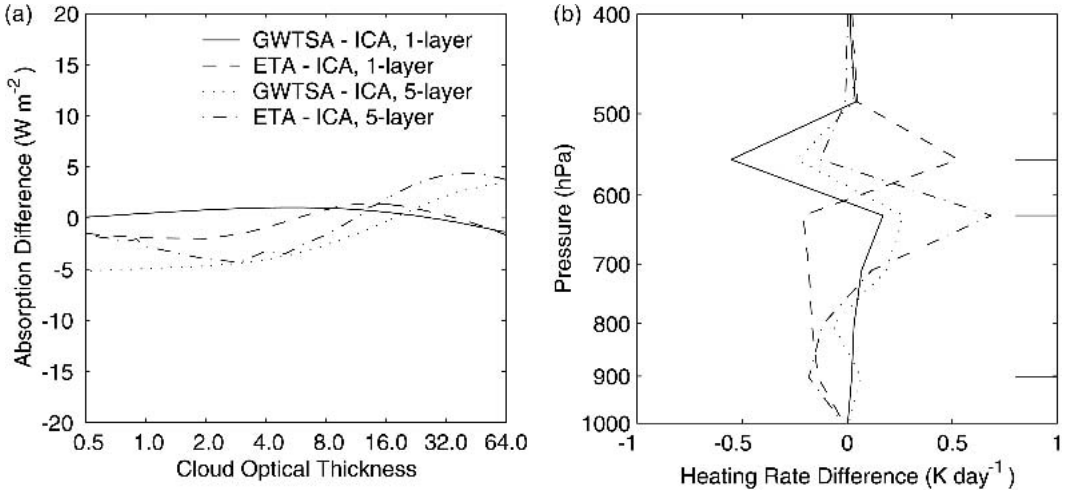

FIG. 6. (a) Error in the irradiance absorbed by the atmosphere as a function of cloud optical thickness and (b) the heating rate error caused by the gamma-weighted two-stream approximation with a one-layer cloud (solid line), with a five-layer cloud (dotted line), by the effective thickness approximation with a one-layer cloud (dashed line), and with a five-layer cloud (dashed–dotted line). The solar zenith angle is 30° and $\nu = 1$. The cloud optical thickness of 64 is used for (b). The horizontal lines on the right side indicate the height of cloud top and cloud base of one- and four-layer clouds.

by the gamma-weighted two-stream approximation reduces to 2.3 W m^{-2} from 6.1 W m^{-2} at 30° solar zenith angle. This indicates that the artifact contributes more than half of the error in the GWTSA results.

The average error caused by the correlation treatment is larger than the average error caused by a gamma distribution approximation; the average albedo error for a cloud with $\bar{\tau} \approx 30$ and $\nu = 1$ is about 0.017 at 30° solar zenith angle and 0.01 at 60° when the cloud is divided into four or five layers. Four to five computational layers with $\bar{\tau} \approx 30$ and $\nu \approx 1$ cases are likely to be for high and midlevel clouds. Because optically thick clouds tend to be horizontally uniform (i.e., a larger ν), a limited number of footprints have these cloud properties. Overcast footprints that have $\bar{\tau} > 20$ and $\nu < 2$ make up 4% of all overcast footprints in the 30 months

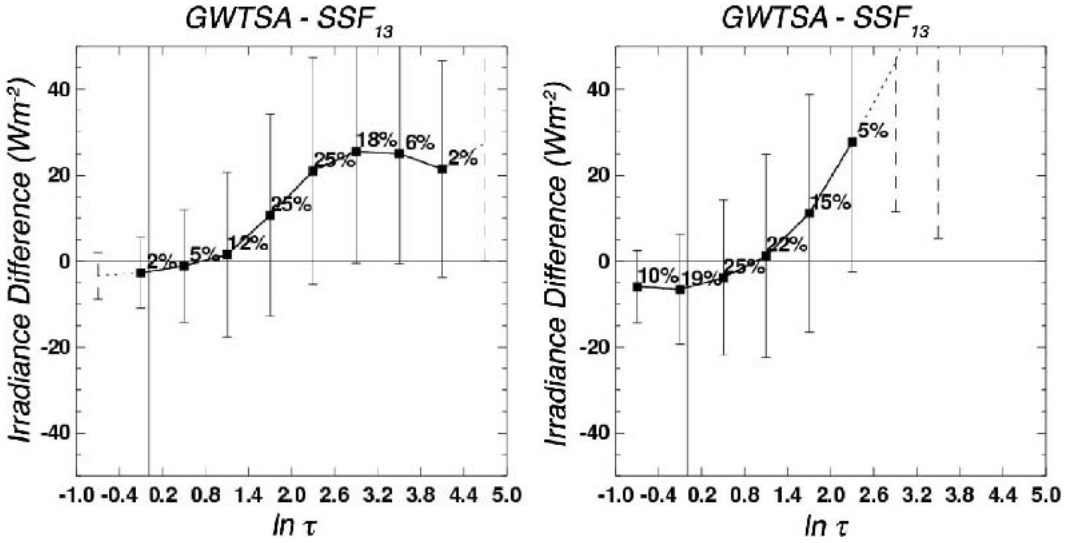

FIG. 7. The top-of-atmosphere irradiance error caused by the gamma-weighted two-stream approximation for (left) overcast cases and (right) partly cloudy cases with clouds extending four computational layers. The cloud optical thicknesses are derived from MODIS radiances over a CERES footprint. The cloud top and base are 5 and 1 km, respectively. The solar zenith angle is 30°. The error bar indicates the standard deviation and the numbers in the figure indicate the percentage of the population.

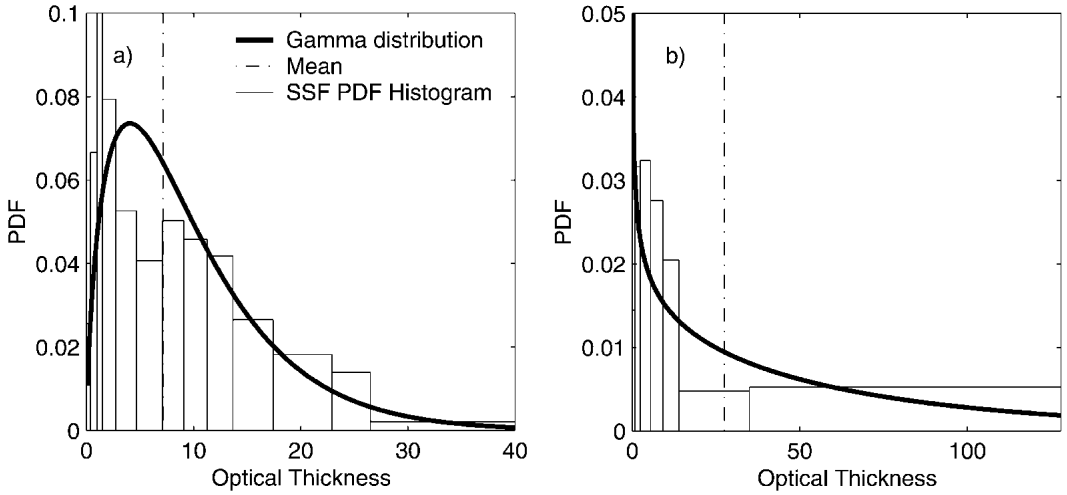

FIG. 8. Optical thickness probability density function from two footprints. The number of subgrid columns in each bin is divided by the width of the bin so that the area is proportional to the number of counts in the bin. Thick solid line is a gamma distribution obtained by the maximum likelihood method of Greenwood and Durand (1960). The vertical dashed–dotted line indicates the mean optical thickness computed by $\exp(\overline{\ln\tau})$.

of CERES data and 0.9% in the dataset used in these computations. Partly cloudy footprints that have these properties are much less; they are 0.6% of all pertly cloudy footprints in 30 months of CERES data and 0.2% in the dataset used in the computations. The primary reason that the gamma-weighted two-stream approximation performs better for partly cloudy footprints is that clouds in partly cloudy footprints tend to be optically thinner than those in overcast footprints.

The average error caused by the effective thickness approximation for overcast clouds is 0.5 W m^{-2} at 30° solar zenith angle and 3.7 W m^{-2} at 60°. The error caused by the approximation depends strongly on optical thickness, but the error at small $\bar{\tau}$ cancels out the error at large $\bar{\tau}$. Because large $\bar{\tau}$ is absent from partly cloudy footprints, the average error caused by the effective thickness approximation is larger for the partly cloudy cases than the overcast cases. The average error by the effective thickness approximation under partly cloudy conditions is -21.5 and -8.2 W m^{-2}, for 30° and 60° solar zenith angles, respectively. Because irradiances are only calculated for a cloudy part of the partly cloudy scenes and the cloud fraction is not accounted for, the actual average error for all sky conditions is smaller than these values. The average error caused by the effective thickness approximation under all sky conditions is potentially larger than the average error caused by the gamma-weighted two-stream approximation because two-thirds of all cloudy footprints are partly cloudy (Table 1).

The accuracy of the effective thickness approximation depends on the magnitude of the higher-order terms of a Taylor expansion because it neglects higher-order terms regardless of their magnitude. An optical thickness range that produces small higher-order terms is narrow compared with the actual variation of cloud optical thickness; Barker (1996) suggests that the range is $5 \le e^{\overline{\ln\tau}}/\mu_0 \le 15$. This can be understood if we assume, following Cahalan et al. (1994a), that the albedo function is given by

$$R(\gamma) = \frac{\gamma\tau/\mu_0}{1 + \gamma\tau/\mu_0}. \tag{14}$$

The second derivative of R with respect to $\ln\tau$ is proportional to $1 - \gamma\tau/\mu_0$. Because the value of γ is approximately 0.1 (King and Harshvardhan 1986; Cahalan et al. 1994a; Bohren 1987), the second derivative is negligible if τ/μ_0 is close to 10. As a consequence, the error caused by the effective thickness approximation is small when τ/μ_0 is distributed around 10. In addition, the contour of the albedo as a function of two parameters for a gamma distribution, the mean optical thickness and shape factor, is shown in Fig. 9. The solid lines in Fig. 9 correspond to the logarithmic average of the optical thickness for a given gamma-distribution computed by Eq. (D3). If a solid line follows a dashed–dotted line, the albedo does not change by changing the shape factor so that the error by the effective optical thickness approximation is small. The dotted line indicates the optical thickness satisfying $\exp(\overline{\ln\tau})/\mu_0 = 10$ for $\mu_0 = 0.87$. It is almost follows the albedo contour, which also indicates that the error by the effective thickness approximation is small if τ/μ_0 is close to 10. Note that the albedo error by the plane parallel homogeneous approximation is obtained by following a vertical line from $\nu = 100$ in Fig. 9. It shows that the error increases especially $\nu < 3$ and $\bar{\tau} > 7$ because the albedo decreases with decreasing the shape factor.

The gamma-weighted two-stream approximation

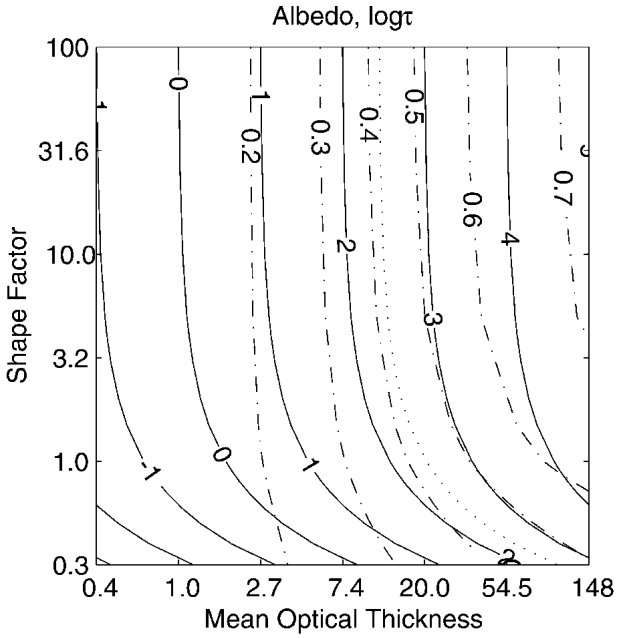

FIG. 9. Albedo as a function of two gamma distribution parameters, mean optical thickness of clouds and shape factor (dashed–dotted lines). The solar zenith angle of 30° and surface albedo of 0.06 are used to compute the albedo. Contour of the logarithmic mean of the optical thickness [$\exp(\overline{\ln\tau})$] corresponding to the gamma distribution is also shown by solid lines. The dotted line indicates the logarithmic mean of the optical thickness that satisfies $\exp(\overline{\ln\tau})/\mu_0 = 10$.

produces smaller bias errors than the effective thickness approximation for thin and very thick clouds, but the albedo bias could be nearly 0.02 for $\bar{\tau} \approx 30$ and $\nu = 1$ at small solar zenith angles depending on the number of computational layers dividing the cloud. The effective thickness approximation produces a small albedo bias error when $\bar{\tau}/\mu_0 \approx 10$, but it can be larger than 0.02 outside this range. Recently Pincus et al. (2003) have demonstrated that if cloud optical thickness is randomly chosen from the distribution in the domain for irradiance computations and the resulting irradiances are averaged over many cases, the bias error of the irradiance vanishes. For comparison to the approximations used in this study, we use a random number generator to pick an optical thickness from SSF_{13}. If the random number is 0.6, for example, we pick the optical thickness corresponding to the cumulative distribution at 0.6 for the irradiance computation, so that the optical thickness distribution used for the computation is statistically equal to the actual optical thickness distribution when many cases are averaged. We then use a homogeneous cloud to compute the irradiance (random method). The results for using the same set of CERES data used in the previous sections are shown in Fig. 10. As expected, the bias error almost vanishes with about 30 000 computations for overcast cases and about 45 000 computations for partly cloudy cases, but the standard deviation is 4 times larger than that from either the gamma-weighted two-steam approximation or effective thickness approximation. The standard deviation produced by the random method is determined by the cloud optical thickness distribution; the wider the cloud optical thickness distribution is, the larger the standard deviation of the irradiances produced by the random method.

All three approximations tested in this study have advantages and disadvantages. The simple effective thickness approximation works in a certain range of optical thicknesses, while the more complicated gam-

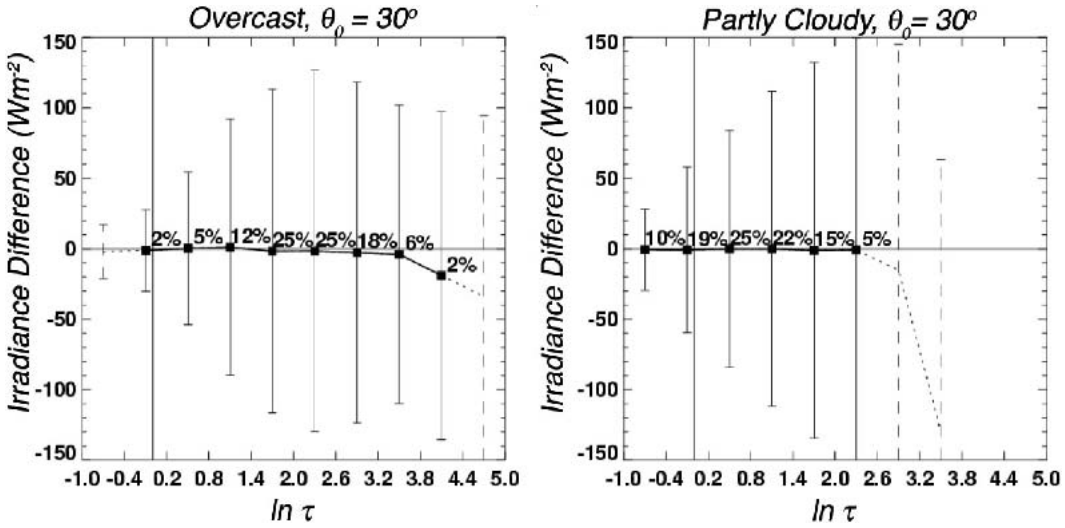

FIG. 10. The top-of-atmosphere irradiance error by the random method for (left) overcast cases and (right) partly cloudy cases. The cloud optical thicknesses are derived from MODIS radiances over a CERES footprint. The cloud top and base are 2 and 1 km, respectively. The solar zenith angle is 30°. The error bar indicates the standard deviation and the numbers in the figure indicate the percentage of the population.

ma-weighted two-stream approximation produces a smaller error for a wider range. Because the gamma-weighted two-stream approximation relies on two parameters derived from retrieved cloud optical thicknesses, it is more affected by the error and approximations in the retrieval algorithm than is the effective thickness approximation. For example, this study indicates that the maximum optical thickness in the retrieval affects the error caused by the gamma-weighted two-stream approximation, but it does not affect the error caused by the effective thickness approximation very much. In addition, for a given measured radiance from an imager the assumption of the cloud particles phase, either ice or liquid water, changes the retrieved optical thickness by almost a factor of 2. Therefore, if both ice and liquid water clouds exist in a footprint, the optical thickness distribution is sometimes bimodal, one mode representing a liquid water cloud and the other representing an ice cloud. A gamma distribution does not represent the histogram very well for mixed phase cases.

The question is then how large these average errors caused by assumptions in the models are compared to errors introduced by other uncertainties. The error in an irradiance computation is also caused by the uncertainty in the inputs. According to Zhang et al. (1995), who computed the irradiance in 2.5° by 2.5° grids and averaged to obtain the global mean, the uncertainty in the daily averaged top-of-atmosphere upward (surface downward) irradiance caused by the uncertainty in the cloud fraction estimate in ISCCP data is 10.3 W m^{-2} (-12.1 W m^{-2}). The uncertainty in the top-of-atmosphere upward (surface downward) broadband shortwave irradiance caused by the uncertainty in the surface albedo is -12.6 W m^{-2} (-2.6 W m^{-2}). By their estimate, the cloud fraction uncertainty is about 10% and the uncertainty in the surface albedo is primarily in estimating land surface albedos. In their sensitivity study, the cloud amount was increased by 22.8%, which is twice the uncertainty of the retrieved cloud amounts, from 47.6% to 70.4%. In addition to these sensitivities, when the cloud optical thickness was changed by 20% from a global mean value of 7.27 to 8.24, the top-of-atmosphere irradiance increased by 4.9 W m^{-2} (Zhang et al. 1995).

If we assume that the average error in the albedo caused by the gamma-weighted two-stream approximation does not depend very much on the solar zenith angle, the daily average error is less than 2 W m^{-2} under all sky conditions. For this estimate, we used an albedo error of 0.012 for overcast conditions and of 0.0009 multiplied by the cloud fraction of 0.59 for partly cloudy conditions. Then these numbers were weighted by the frequencies of occurrence shown in Table 1 to obtain the error under all sky conditions. The corresponding error caused by the effective thickness approximation is also less than 2 W m^{-2}. Although the error estimate by Zhang et al. (1995) seems to be an upper bound, the error in the top-of-atmosphere and surface irradiances under all sky conditions caused by these approximations is smaller than the uncertainty caused by input errors alone determined by Zhang et al. (1995).

7. Conclusions

Two sources of error caused by the gamma-weighted two-stream approximation considered in this study are 1) assumption of a gamma distribution of cloud optical thickness and 2) treatment of vertical correlation of cloud properties. The error caused by a gamma distribution approximation is due to the deviation of the actual distribution from a gamma distribution and by the fact that retrieved cloud optical thicknesses have a maximum value. Because there is a maximum value in the retrieval but the approximation assumes the distribution is 0 to infinity, it tends to overestimate the top-of-atmosphere irradiance when the average optical thickness is close to the maximum value. In addition, the method used to obtain the histogram in the SSF product affects the gamma distribution estimate when a footprint contains a small fraction of thin clouds and a large fraction of thick clouds. This artifact contributes nearly half of the average error caused by the gamma-weighted two-stream approximation when the clouds are in one computational layer. These results imply that irradiance computations using the gamma-weighted two-stream approximation are affected more by cloud retrieval errors than those using the effective thickness approximation. The average error in the top-of-atmosphere irradiance caused by the gamma distribution approximation is 6.1 W m^{-2} at 30° solar zenith angle and 4.0 W m^{-2} at 60° solar zenith angle under overcast conditions.

The average error caused by the correlation treatment is larger; the average error in the irradiance at the top-of-atmosphere is 8.6 W m^{-2} at 30° solar zenith angle under overcast conditions when a cloud layer is divided into four computational layers. The error caused by the correlation treatment could go up to 25–30 W m^{-2} at 30° solar zenith angle and 10–15 W m^{-2} at 60° when a cloud layer of $\bar{\tau} \approx 30$ and $\nu = 1$ is divided into 10 computational layers. Physically thick and horizontally inhomogeneous clouds are affected by the error; CERES footprints that have $\bar{\tau} > 20$ and $\nu < 2$ are about 4% of all overcast footprints and 0.6% of all partly cloudy footprints in the 30 months of CERES data. The average error caused by the gamma-weighted two-stream approximation is smaller for partly cloudy conditions than overcast clouds. Because clouds under partly cloudy conditions are optically thinner, the errors described above do not affect them as much as for overcast clouds.

The error caused by the effective thickness approximation is small when $\bar{\tau}/\mu_0 \approx 10$. When the top-of-

atmosphere irradiance is computed using the approximation, the model underestimates (overestimates) albedo when the optical thickness is below (above) this range. Because the error at smaller optical thicknesses cancels out the error at larger optical thicknesses, the average error caused by the approximation for overcast clouds is 0.5 and 3.9 W m^{-2} at solar zenith angles of 30° and 60°, respectively. The average error under partly cloudy conditions is larger than overcast cases because of the absence of optically thick clouds in partly cloudy scenes. When these errors are converted to a daily mean value at the top of the atmosphere, it is less than 2 W m^{-2} for both caused by the gamma-weighted two-stream and effective thickness approximations. The error in the top-of-atmosphere and surface irradiances caused by these approximations is smaller than the error caused by the uncertainty in the inputs used for radiation budget estimate such as cloud fraction, surface albedo, and cloud optical thickness.

Acknowledgments. We are grateful to Dr. H. W. Barker at Environment Canada for useful suggestions earlier in the course of this work, to Dr. L. M. Hinkelman for an extensive review of the manuscript, and to Dr. Oreopoulos for useful discussions. We also thank two anonymous reviewers for helpful comments. The work is supported by NASA through the Clouds and the Earth's Radiant Energy System (CERES) project Grant NAG-1-2318.

APPENDIX A

Expression of Diffuse Irradiance

When the distribution of cloud optical thickness of the cloud layer follows a gamma distribution, the upward irradiance F^+ and downward irradiance F^- at the bottom of the jth layer can be written as (Kato 2003)

$$F_j^+(\xi) = E_{13j}^-(\xi) + E_{24j}^-(\xi) - W_{13j}^-(\xi)F_{j-1}^-(1) - W_{24j}^-(\xi)F_j^+(1) + C_j^+(\xi), \quad \text{(A1)}$$

and

$$F_j^-(\xi) = E_{13j}^+(\xi) + E_{24j}^+(\xi) - W_{13j}^+(\xi)F_{j-1}^-(1) - W_{24j}^+(\xi)F_j^+(1) + C_j^-(\xi), \quad \text{(A2)}$$

where

$$E_{13j}^+(\xi) = e_{1j}^c\eta_j + e_{3j}^c, \quad \text{(A3)}$$

$$E_{24j}^+(\xi) = e_{4j}^c\eta_j + e_{2j}^c, \quad \text{(A4)}$$

$$W_{13j}^+(\xi) = e_{1j}^w\eta_j + e_{3j}^w, \quad \text{(A5)}$$

$$W_{24j}^+(\xi) = e_{4j}^w\eta_j + e_{2j}^w, \quad \text{(A6)}$$

$$E_{13j}^-(\xi) = e_{1j}^c + e_{3j}^c\eta_j, \quad \text{(A7)}$$

$$E_{24j}^-(\xi) = e_{4j}^c + e_{2j}^c\eta_j, \quad \text{(A8)}$$

$$W_{13j}^-(\xi) = e_{1j}^w + e_{3j}^w\eta_j, \quad \text{(A9)}$$

$$W_{24j}^-(\xi) = e_{4j}^w + e_{2j}^w\eta_j, \quad \text{(A10)}$$

$$e_{1j}^c(\xi) = \sum_{i=1}^{\infty} \frac{\eta_j^{2i-1}C_j^-(0)}{\left[1 + (2i - \xi)\dfrac{\lambda_j\bar{\tau}_j}{\nu_j}\right]^{\nu_j}}, \quad \text{(A11)}$$

$$e_{2j}^c(\xi) = \sum_{i=1}^{\infty} \frac{\eta_j^{2i-1}C_j^+(0)}{\left\{1 + \left[\dfrac{1}{\mu_0} + (2i - 1 + \xi)\lambda_j\right]\dfrac{\bar{\tau}_j}{\nu_j}\right\}^{\nu_j}}, \quad \text{(A12)}$$

$$e_{3j}^c(\xi) = -\sum_{i=1}^{\infty} \frac{\eta_j^{2(i-1)}C_j^-(0)}{\left\{1 + [2(i-1) + \xi]\dfrac{\lambda_j\bar{\tau}_j}{\nu_j}\right\}^{\nu_j}}, \quad \text{(A13)}$$

$$e_{4j}^c(\xi) = -\sum_{i=1}^{\infty} \frac{\eta_j^{2(i-1)}C_j^+(0)}{\left\{1 + \left[\dfrac{1}{\mu_0} + (2i - 1 - \xi)\lambda_j\right]\dfrac{\bar{\tau}_j}{\nu_j}\right\}^{\nu_j}}, \quad \text{(A14)}$$

$$e_{1j}^w(\xi) = \sum_{i=1}^{\infty} \frac{\eta_j^{2i-1}}{\left[1 + (2i - \xi)\dfrac{\lambda_j\bar{\tau}_j}{\nu_j}\right]^{\nu_j}}, \quad \text{(A15)}$$

$$e_{2j}^w(\xi) = \sum_{i=1}^{\infty} \frac{\eta_j^{2i-1}}{\left[1 + (2i - 1 + \xi)\dfrac{\lambda_j\bar{\tau}_j}{\nu_j}\right]^{\nu_j}}, \quad \text{(A16)}$$

$$e_{3j}^w(\xi) = -\sum_{i=1}^{\infty} \frac{\eta_j^{2(i-1)}}{\left\{1 + [2(i-1) + \xi]\dfrac{\lambda_j\bar{\tau}_j}{\nu_j}\right\}^{\nu_j}}, \quad \text{(A17)}$$

$$e_{4j}^w(\xi) = -\sum_{i=1}^{\infty} \frac{\eta_j^{2(i-1)}}{\left[1 + (2i - 1 - \xi)\dfrac{\lambda_j\bar{\tau}_j}{\nu_j}\right]^{\nu_j}}, \quad \text{(A18)}$$

$$C_j^+(\xi) \frac{\bar{\omega}_j F_j^d(\xi)[(\gamma_{1j} - 1/\mu_0)\gamma_{3j} + \gamma_{2j}\gamma_{4j}]}{\mu_0\lambda_j^2 - 1/\mu_0}, \quad \text{(A19)}$$

$$C_j^-(\xi) \frac{\bar{\omega}_j F_j^d(\xi)[(\gamma_{1j} + 1/\mu_0)\gamma_{4j} + \gamma_{2dj}\gamma_{3j}]}{\mu_0\lambda_j^2 - 1/\mu_0}, \quad \text{(A20)}$$

$$\eta = \frac{\gamma_2}{\gamma_1 + \lambda}, \quad \text{(A21)}$$

$$\lambda = (\gamma_1^2 - \gamma_2^2)^{1/2}. \quad \text{(A22)}$$

In these equations, $\xi = 0$ and $\xi = 1$ indicate at the top and bottom of the cloud layer, respectively, $\bar{\omega}$ is the single scattering albedo, F_j^d is the direct irradiance, and γ_1, γ_2, γ_3, and γ_4 are coefficients that depend on the

form of the two-stream approximation (e.g., Meador and Weaver 1980). Note that Eqs. (33b) and (33d) in Kato (2003) have an extra $1/\mu_0$ in the denominator that should be eliminated.

If $F_j^d(0)$ is proportional to $\exp(-C\tau_j/\mu_0)$ and the diffuse irradiance $F_{j-1}^-(1)$ is assumed to be proportional to $\exp[-0.063C(2-\mu_0)\tau]$ (Oreopoulos and Barker 1999), where C is give by (4), then equations (A11) to (A 14), (A 15), and (A 17) become

$$e_{1j}^c(\xi) = \sum_{i=1}^{\infty} \frac{A\eta_j^{2i-1} C_j^-(0)}{\left[1 + \frac{C\bar{\tau}_j}{\nu\mu_0} + (2i-\xi)\frac{\lambda_j\bar{\tau}_j}{\nu_j}\right]^{\nu_j}}, \tag{A23}$$

$$e_{2j}^c(\xi) = \sum_{i=1}^{\infty} \frac{A\eta_j^{2i-1} C_j^+(0)}{\left\{1 + \frac{C\bar{\tau}_j}{\nu\mu_0} + \left[\frac{1}{\mu_0} + (2i-1+\xi)\lambda_j\right]\frac{\bar{\tau}_j}{\nu_j}\right\}^{\nu_j}}, \tag{A24}$$

$$e_{3j}^c(\xi) = -\sum_{i=1}^{\infty} \frac{A\eta_j^{2(i-1)} C_j^-(0)}{\left\{1 + \frac{C\bar{\tau}_j}{\nu\mu_0} + [2(i-1)+\xi]\frac{\lambda_j\bar{\tau}_j}{\nu_j}\right\}^{\nu_j}}, \tag{A25}$$

$$e_{4dj}^c(\xi) = -\sum_{i=1}^{\infty} \frac{A\eta_j^{2(i-1)} C_j^+(0)}{\left\{1 + \frac{C\bar{\tau}_j}{\nu\mu_0} + \left[\frac{1}{\mu_0} + (2i-1-\xi)\lambda_j\right]\frac{\bar{\tau}_j}{\nu_j}\right\}^{\nu_j}}, \tag{A26}$$

where $A = (1 + C\bar{\tau}_j/\nu\mu_0)^{\nu}$, and

$$e_{1j}^w(\xi) = \sum_{i=1}^{\infty} \frac{B\eta_j^{2i-1}}{\left[1 + \frac{D\bar{\tau}_j}{\nu} + (2i-\xi)\frac{\lambda_j\bar{\tau}_j}{\nu_j}\right]^{\nu_j}}, \tag{A27}$$

$$e_{3j}^w(\xi) = -\sum_{i=1}^{\infty} \frac{B\eta_j^{2(i-1)}}{\left\{1 + \frac{D\bar{\tau}_j}{\nu} + [2(i-1)+\xi]\frac{\lambda_j\bar{\tau}_j}{\nu_j}\right\}^{\nu_j}}, \tag{A28}$$

where $B = (1 + D\bar{\tau}_j/\nu)^{\nu}$ and $D = 0.063C(2 - \mu_0)$.

APPENDIX B

Effect of the Delta Approximation

A two-stream approximation is usually combined with the delta approximation (Joseph et al. 1976) to reduce the error in the total (direct irradiance plus diffuse) irradiance. One subtle adjustment associated with the delta approximation in computing C given by (9) is that the direct irradiance incident on the lower layer needs to include the direct radiation scattered in the forward direction in the upper layer. Therefore, (9) is replaced by

$$C = \eta(1 - \omega_u g_u^2)\bar{\tau}_u/\bar{\tau}, \tag{B1}$$

where $1 - \omega_u g_u^2$ is the correction factor to the optical thickness using the delta approximation, ω_u is the single scattering albedo of the upper layer and g_u is the asymmetry parameter of the upper layer. When the delta approximation is applied to the optical thickness of the lower layer, the same factor is multiplied to the numerator such that

$$C = \eta(1 - \omega g^2)\bar{\tau}_u'/\bar{\tau}', \tag{B2}$$

where $\bar{\tau}_u'$ and $\bar{\tau}'$ is the optical thickness with the delta approximation; C is, therefore, unaltered by the delta approximation when it is applied to the lower layer. The value C by (B1) is used when the total irradiance is computed, but (9) is used for the direct irradiance computation.

APPENDIX C

Finite Maximum Optical Thickness Case

When the optical thickness distribution is from 0 to a finite optical thickness τ_m, each term in the summation appears in (A11)–(A18) and (A23)–(A28) needs to be multiplied by

$$\frac{\gamma\left(\nu_j, \phi_i \frac{\nu_j}{\bar{\tau}}\tau_m\right)}{\gamma\left[\nu, \tau_m\left(\frac{\nu}{\bar{\tau}} + D\right)\right]}, \tag{C1}$$

such that

$$e_{kj}'^{y}(\xi) = \sum_{i=1}^{\infty} \frac{\gamma\left(\nu_j, \phi_i \frac{\nu_j}{\bar{\tau}}\tau_m\right)}{\gamma\left[\nu, \tau_m\left(\frac{\nu}{\bar{\tau}} + D\right)\right]} e_{kj}^y(\xi); \tag{C2}$$

here ϕ_i indicates the expression inside the brackets of power of ν_i in the denominator [e.g., $\phi_i = 1 + (2i - \xi)\lambda_j\bar{\tau}_j/\nu_j$ for e_{1j}^c] and the superscript y is either c or w. $\gamma(\alpha, x)$ in the above expression is the incomplete gamma function defined as

$$\gamma(\alpha, x) = \int_0^x e^{-t} t^{\alpha-1} dt.$$

The difference in the irradiance with and without this correction becomes significant when the optical thickness is slightly less than τ_m (Fig. C1).

APPENDIX D

Relation between the Shape Factor and Scaling Factor

The derivation of the relation between the shape factor of a gamma distribution ν and scaling factor χ of the effective thickness approximation that is defined by

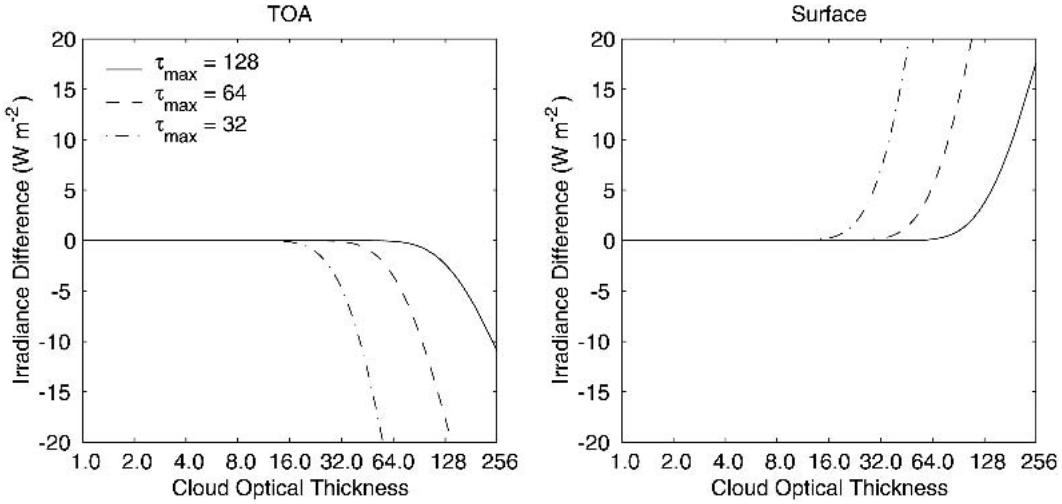

FIG. C1. Broadband irradiance difference at the top of the atmosphere and surface computed with applying correction of the incomplete gamma function and without the correction. The difference is obtained by subtracting the irradiance without the correction from that with the correction. Different lines indicate results of different maximum optical thicknesses used in the incomplete gamma function. The solar zenith angle is 30° and surface albedo is 0.06.

$$\chi = \exp(\overline{\ln\tau} - \ln\bar{\tau}) \tag{D1}$$

is given by Barker (1996), but a straightforward derivation is given here. The logarithmic average of optical thickness $\overline{\ln\tau}$ is

$$\overline{\ln\tau} = \int_{-\infty}^{\infty} \frac{dn}{d\ln\tau} \ln\tau \, d\ln\tau = \int_{0}^{\infty} \frac{dn}{d\tau} \ln\tau \, d\tau, \tag{D2}$$

where $dn/d\ln\tau$ and $dn/d\tau$ is the probability density function of the optical thickness distribution. When the gamma distribution by (D2) is substituted for $dn/d\tau$, (D2) leads to (Gradshteyn and Ryzhik 1965)

$$\overline{\ln\tau} = \psi(\nu) + \ln\bar{\tau} - \ln\nu, \tag{D3}$$

where ψ is the psi function defined as $\psi(z) = d\ln\Gamma(z)/dz$ and $\Gamma(z)$ is the gamma function defined as $\Gamma(z) = \int_0^\infty e^{-t}t^{z-1}dt$. This leads to

$$\chi = \frac{\exp[\psi(\nu)]}{\nu} \tag{D4}$$

This gives the reason for the method of estimating shape factor by (8), (9), and (10); $\overline{\ln\tau} - \ln\bar{\tau}$ is a function of ν alone when the distribution is assumed to be a gamma distribution. An approximate relation between χ and ν is given by Rossow et al. (2002).

REFERENCES

Barker, H. W., 1996: A parameterization for computing grid-averaged solar fluxes for inhomogeneous marine boundary layer clouds. Part I: Methodology and homogeneous biases. *J. Atmos. Sci.,* **53,** 2289–2303.

——, and Q. Fu, 2000: Assessment and optimization of the gamma-weighted two-stream approximation. *J. Atmos. Sci.,* **57,** 1181–1188.

——, B. A. Wielicki, and L. Parker, 1996: A parameterization for computing grid-averaged solar fluxes for inhomogeneous marine boundary layer clouds. Part II: Validation using satellite data. *J. Atmos. Sci.,* **53,** 2304–2316.

——, and Coauthors, 2003: Assessing 1D atmospheric solar radiative transfer models: Interpretation and handling of unresolved clouds. *J. Climate,* **16,** 2676–2699.

Barkstrom, B. B., 1984: The Earth Radiation Budget Experiment (ERBE). *Bull. Amer. Meteor. Soc.,* **65,** 1170–1185.

Bohren, C. F., 1987: Multiple scattering of light and some of its observable consequences. *Amer. J. Phys.,* **27,** 2502–2509.

Cahalan, R. T., W. Ridgway, W. J. Wiscombe, T. L. Bell, and J. B. Snider, 1994a: The albedo of fractal stratocumulus clouds. *J. Atmos. Sci.,* **51,** 2434–2455.

——, ——, ——, S. Gollmer, and Harshvardhan, 1994b: Independent pixel and Monte Carlo estimate of stratocumulus albedo. *J. Atmos. Sci.,* **51,** 3776–3790.

Cairns, B., A. A. Lacie, and B. E. Carlson, 2000: Absorption within inhomogeneous clouds and its parameterization in general circulation models. *J. Atmos. Sci.,* **57,** 700–714.

Charlock, T. P., and T. L. Alberta, 1996: The CERES/ARM/GEWEX experiment (CAGEX) for the retrieval of radiative fluxes with satellite data. *Bull. Amer. Meteor. Soc.,* **77,** 2673–2683.

Geier, E. B., R. N. Green, D. P. Kratz, P. Minnis, W. Miller, S. K. Nolan, and C. B. Franklin, cited 2002: Clouds and earth's radiant energy system single satellite footprint TOA/surface flux and clouds (SSF) collection document. [Available online at http://earth-www.larc.nasa.gov/ssf.]

Gradshteyn, I. S., and I. M. Ryzhik, 1965: *Table of Integrals, Series, and Products.* 4th ed. Academic Press, 1086 pp. (Translated by A. Jeffery.)

Greenwood, J. A., and D. Durand, 1960: Aids for fitting the gamma distribution by maximum likelihood. *Technometrics,* **2,** 55–65.

Hu, Y. X., and K. Stamnes, 1993: An accurate parameterization of the radiative properties of water clouds suitable for use in climate models. *J. Climate,* **6,** 728–742.

Joseph, J. H., W. J. Wiscombe, and J. A. Weinman, 1976: The delta-Eddington approximation for radiative flux transfer. *J. Atmos. Sci.,* **33,** 2452–2459.

Kato, S., 2003: Computation of domain-averaged shortwave irradiance by a one-dimensional algorithm incorporating correlations between optical thickness and direct incident radiation. *J. Atmos. Sci.,* **60,** 182–193.

——, T. P. Ackerman, J. H. Mather, and E. E. Clothiaux, 1999: The *k*-distribution method and correlated-*k* approximation for a Shortwave Radiative Transfer Model. *J. Quant. Spectrosc. Radiat. Transfer,* **62,** 109–121.

King, M. D., and Harshvardhan, 1986: Comparative accuracy of selected multiple scattering approximations. *J. Atmos. Sci.,* **43,** 784–801.

——, Y. J. Kaufman, W. P. Menzel, and D. Tanre, 1992: Remote sensing of cloud, aerosol, and water vapor properties from the Moderate resolution Imaging Spectrometer (MODIS). *IEEE Trans. Geosci. Remote Sens.,* **30,** 2–27.

Loeb, N. G., N. Manalo-Smith, S. Kato, W. F. Miller, S. K. Gupta, P. Minnis, and B. A. Wielicki, 2003: Angular distribution models for top-of-atmosphere radiative flux estimation from the clouds and the Earth's Radiant Energy System instrument on the Tropical Rainfall Measuring Mission satellite. Part I: Methodology. *J. Appl. Meteor.,* **42,** 240–265.

McClatchey, R. A., R. W. Fenn, J. E. A. Selby, F. E. Volz, and J. S. Garing, 1972: Optical properties of the atmosphere. 3d ed. Environmental Research Paper 411, Air Force Cambridge Research Laboratory, Bedford, MA, 110 pp.

Meador, W. E., and W. R. Weaver, 1980: Two-stream approximation to radiative transfer in planetary atmospheres: A unified description of existing methods and new improvement. *J. Atmos. Sci.,* **37,** 630–643.

Minnis, P., D. P. Garber, D. F. Young, R. F. Arduni, and Y. Takano, 1998: Parameterization of reflectance and effective emittance for satellite remote sensing of cloud properties. *J. Atmos. Sci.,* **55,** 3313–3339.

Oreopoulos, L., and R. Davies, 1998: Plane parallel albedo biases from satellite observations. Part II: Parameterizations for bias removal. *J. Climate,* **11,** 933–944.

——, and H. W. Barker, 1999: Accounting for subgrid-scale cloud variability in a multi-layer 1D solar radiative transfer algorithm. *Quart. J. Roy. Meteor. Soc.,* **125,** 301–330.

Pincus, R., H. W. Barker, and J.-J. Morcrette, 2003: A fast, flexible, approximate technique of computing radiative transfer for inhomogeneous clouds. *J. Geophys. Res.,* **108,** 4376, doi:10.1029/2002JD003322.

Rossow, W. B., and R. A. Schiffer, 1991: ISCCP cloud data products. *Bull. Amer. Meteor. Soc.,* **72,** 2–20.

——, and Y.-C. Zhang, 1995: Calculation of surface and top of atmosphere radiative fluxes from physical quantities based on ISCCP data sets: 2. Validation and first results. *J. Geophys. Res.,* **100,** 1167–1198.

——, C. Delo, and B. Cairns, 2002: Implications of the observed mesoscale variations of clouds for the earth's radiation budget. *J. Climate,* **15,** 557–585.

Smith, G. L., R. N. Green, E. Raschke, L. M. Avis, J. T. Suttles, B. A. Wielicki, and R. Davies, 1986: Inversion methods for satellite studies of the earth's radiation budget: Development of algorithms for the ERBE mission. *Rev. Geophys.,* **24,** 407–421.

Thom, H. C. S., 1958: A note on the gamma distribution. *Mon. Wea. Rev.,* **86,** 117–122.

Wielicki, B. A., B. R. Barkstrom, E. F. Harrison, B. B. Lee III, G. L. Smith, and J. E. Cooper, 1996: Clouds and the Earth's Radiant Energy System (CERES): An Earth Observing System experiment. *Bull. Amer. Meteor. Soc.,* **77,** 853–868.

Zhang, T.-C., W. B. Rossow, and A. A. Lacis, 1995: Calculation of surface and top of atmosphere radiation fluxes from physical quantities based on ISCCP data sets: 1. Method and sensitivity to input data uncertainties. *J. Geophys. Res.,* **100,** 1149–1165.